ELSEVIER

Journal of Hazardous Materials B94 (2002) 63–88

Journal of Hazardous Materials

www.elsevier.com/locate/jhazmat

Study of the physical and chemical mechanisms influencing the long-term environmental stability of natrojarosite waste treated by stabilization/solidification

Lionel J.J. Catalan*, Emmanuel Merlière, Christine Chezick

Department of Chemical Engineering, Lakehead University, 955 Oliver Road, P7B 5E1 Thunder Bay, Ont., Canada

Received 24 October 2001; received in revised form 7 March 2002; accepted 7 March 2002

Abstract

Natrojarosite is a residue of zinc refining generated in large quantities by zinc producers in many parts of the world. Stabilization/solidification (s/s) is currently used to immobilize heavy metals prior to storage of the solidified material as a heap. Our study aimed at assessing the long-term environmental stability of treated natrojarosite waste in the field situation. Flow-through leaching tests were carried out on monolithic samples in a modified triaxial cell and on crushed samples in packed columns. Tests with monolithic samples simulated natural infiltration through treated material containing few cracks and fractures, whereas, packed column tests were more representative of weathered material. The microstructure of leached and unleached materials was characterized by scanning electron microscopy and X-ray energy dispersive spectrometry (SEM–EDX). The results of flow-through leaching tests combined with microscopic characterization and geochemical equilibrium calculations provided valuable insights on the physical and chemical mechanisms influencing the long-term leaching behavior. This information was used to develop a mathematical model for alkalinity depletion in the treated waste. When infiltration of acid rain through the material was considered, the model predicted that the leachate would remain at high pH for many thousands of years in the field.

Keywords: Natrojarosite; Stabilization; Solidification; Leaching; Heavy metals; Modeling

* Corresponding author. Tel.: +1-807-343-8573; fax: +1-807-343-8928.
E-mail address: lionel.catalan@lakeheadu.ca (L.J.J. Catalan).

0304-3894/02/$ – see front matter © 2002 Elsevier Science B.V. All rights reserved.
PII: S0304-3894(02)00059-6

1. Introduction

Stabilization/solidification (s/s) processes are applicable to a wide variety of industrial wastes as a treatment step prior to long-term storage on land (Conner and Hoeffner [1]). The main goals of s/s are: (1) to immobilize the contaminants through chemical and physical mechanisms in order to reduce the rate at which contaminants can be transported to the environment; and (2) to increase the structural integrity of the treated material. Inorganic wastes, especially liquids and sludges containing heavy metals, are often treated by addition of alkaline and cementing agents to precipitate the dissolved metals and yield a solid waste form. During solidification, cement hydration reactions produce a calcium–silicate–hydrate (C–S–H) gel named tobermorite, which is responsible for creating filamentous structures that coat and hold the waste particles together.

The waste considered in this paper, natrojarosite, is produced during the refining of zinc concentrates. Pure natrojarosite has the formula $NaFe_3(SO_4)_2(OH)_6$; however, the waste also contains significant concentrations of metal impurities, most notably Zn, Pb, and Cu. Natrojarosite waste is currently treated by a full-scale continuous s/s process in a major zinc refinery located in the Quebec, Canada. In this process, the raw waste is first mixed with lime to precipitate the dissolved metals and then with ordinary portland cement (OPC). The treated waste is deposited as a heap over a natural layer of silty clay in the field, where it is exposed to rain and snow.

A micromineralogical study of s/s treated natrojarosite was carried out by Chen and Dutrizac [2] using scanning electron microscopy combined with energy dispersive X-ray analysis (SEM–EDX), quantitative electron microprobe analysis, and X-ray diffraction (XRD). Results suggested that portland cement reacts to some extent with natrojarosite to form the iron analogue of ettringite [$Ca_6Fe_2(SO_4)_3(OH)_{12}\cdot nH_2O$] together with ferric hydroxide and sodium sulfate. It was also concluded that water soluble Zn in the natrojarosite waste is structurally incorporated in cement reaction products rich in Ca, Al, Fe, Si, and sulfate. Further characterization worked by Ivey [3] using transmission electron microscopy combined with EDX (TEM–EDX) and electron diffraction found three main types of microstructural features in the treated waste: (1) blocky crystals of natrojarosite containing small amounts of Pb, Zn, Ca, and Si; (2) amorphous mesh-like structures consisting of (C–S–H) surrounding the jarosite crystals and also containing small amounts of sorbed Fe, Pb, Zn, S and Na; and (3) fine grained polycrystalline rods identified as gypsum or an ettringite-type phase [$Ca_6Al_2(SO_4)_3(OH)_{12}\cdot nH_2O$] with partial substitution of Fe for Al. No Zn was detected in the ettringite-type phase, in contrast with the results of Chen and Dutrizac [2]. The poorer spatial resolution of SEM–EDX and microprobe analysis relative to TEM was suggested as a likely explanation for this discrepancy.

The chemical stability of s/s treated material is usually evaluated by means of leaching tests. Environmental monitoring of industrial s/s operations is largely based on regulatory static batch leaching tests, such as the toxicity characteristic leaching procedure (TCLP) [4]. These tests are relatively easy to carry out but have several limitations for predicting the long-term leaching characteristics of s/s treated material in the field. Since the leachant is not renewed, static tests only provide one leachate composition corresponding to a single set of leaching conditions. This differs from the situation in the field where natural infiltration water and groundwater in contact with s/s treated material are constantly renewed, thus

progressively removing alkalinity from the solids and, therefore, modifying the leaching conditions over time. In addition, TCLP procedures only specify a maximum particle size for the solids, but studies have shown that the leachate composition is strongly influenced by the size distribution of the particles (Prange and Garvey [5]).

S/s treatment of natrojarosite waste produces a material that is porous and somewhat permeable. Hence, infiltration of rain and snowmelt water through the treated waste occurs, albeit at a slow rate. In the long-term cracks formed by the progressive curing of the treated waste, as well as degradation of the physical characteristics of the material subjected to extreme weathering, may modify the infiltration rates locally in the heap. A realistic assessment of the leaching characteristics of the treated waste in the field over long time periods must, therefore, consider the flow of leachant through the material. Flow-through leaching tests can be carried out on monolithic samples using modified triaxial testing equipment (Butcher et al. [6], Poon et al. [7], Poon and Chen [8]) or on crushed samples (Shackelford and Glade [9], Bishop [10,11]) by means of packed column tests. Both types of tests allow for monitoring the leachate composition versus the volume of leachant passed through the sample. However, the two tests differ in relation to the flow regime of the leachant. Tests carried out on monolithic samples involve leachant flow through most of the sample porosity. As a result, they are more representative of infiltration through material that has never been altered mechanically or by weathering, and which, therefore, exhibits few fractures and little channeling. On the other hand, leachant flow in column tests takes place mostly around the particles of crushed material. Therefore, column tests are better suited to simulate infiltration through cracks and fractures resulting from local weathering of the s/s treated material over time and reworked material not properly compacted.

The objectives of the present study were to characterize the long-term leaching behavior of s/s treated natrojarosite waste by means of flow-through leaching tests on monolithic and crushed samples. The microstructural changes caused by leaching were characterized by SEM–EDX. Potential solubility controls on the leaching behavior were assessed by geochemical equilibrium modeling. A further objective of this study was to develop a mathematical model for alkalinity depletion in the treated material, so as to predict the length of time for which metals will remain effectively immobilized in the field.

2. Experimental methods

2.1. Sample preparation

Natrojarosite sludge containing 59.3% solids and 40.7% liquid by weight was obtained from Canadian Electrolytic Zinc in Valleyfield, Quebec. The elemental compositions of the solid and liquid fractions are given in Table 1. The high Ca concentrations in both phases are explained by the presence of significant quantities of gypsum ($CaSO_4 \cdot 2H_2O$) in the waste. The sludge was first mixed with quicklime (CaO) for 5 min and subsequently with OPC for 30 min. The sequence of treatment steps was consistent with the full-scale s/s process currently in use at the zinc refinery. The dry weight ratios of CaO and OPC to sludge solids were 0.0038 and 0.13, respectively. The mixture was then poured into cylindrical molds made of

Table 1
Elemental composition of solid and liquid fractions of raw natrojarosite waste

Element	Concentration in solids (μg/g)	Concentration in liquid (μg/g)
Al	1748	6.4
Be	59	0.53
Ca	32169	456
Cd	114	62.6
Co	23	0.15
Cr	14	–
Cu	1653	3.3
Fe	317657	1150
K	321	2.0
Mg	110	47.3
Mn	124	33.4
Na	24257	357
Ni	2.8	0.07
Pb	40364	0.13
S	111121	1830
Si	2538	70.4
Zn	18782	320

PVC. Samples were cured at 100% humidity for a minimum of 56 days and a maximum of 178 days before the leaching tests.

The bulk density and porosity of s/s treated natrojarosite were 1.76 g/cm^3 and 59%, respectively. Porosity was determined by comparing the masses of samples of known volumes after immersion in water for 24 h and after overnight drying at 40 °C. The unconfined compressive strength was 1.85 MPa for cylindrical samples measuring 7.6 cm in diameter and 15.2 cm in length.

2.2. Leaching tests

All leaching tests were carried out with a leachant consisting of a buffered acetic acid/sodium acetate solution at pH = 4.93. This solution was identical to extraction fluid #1 described in the TCLP method 1311 [4].

Flow-through leaching tests on monolithic samples were conducted in a modified triaxial cell (Fig. 1). These tests are called "triaxial tests" in the following. Sample dimensions and operating parameters for tests T1–T5 are given in Table 2. The leachant was injected at the bottom of the samples at pressures ranging from 103 to 382 kPa. The leachate was recovered at the top of the samples at atmospheric pressure. A tubular latex membrane was held around the samples by a confining pressure higher than the injection pressure to ensure that all the leachant flowed vertically through the monoliths. Before the start of leachant injection, the samples were evacuated for 2 h by connecting a vacuum pump to the leachate line. This ensured complete saturation of the sample porosity during leaching.

Column leaching tests were carried out in acrylic columns measuring 5.1 cm i.d. and 20.2 cm in height. The leachant was injected at the bottom of the columns by means of

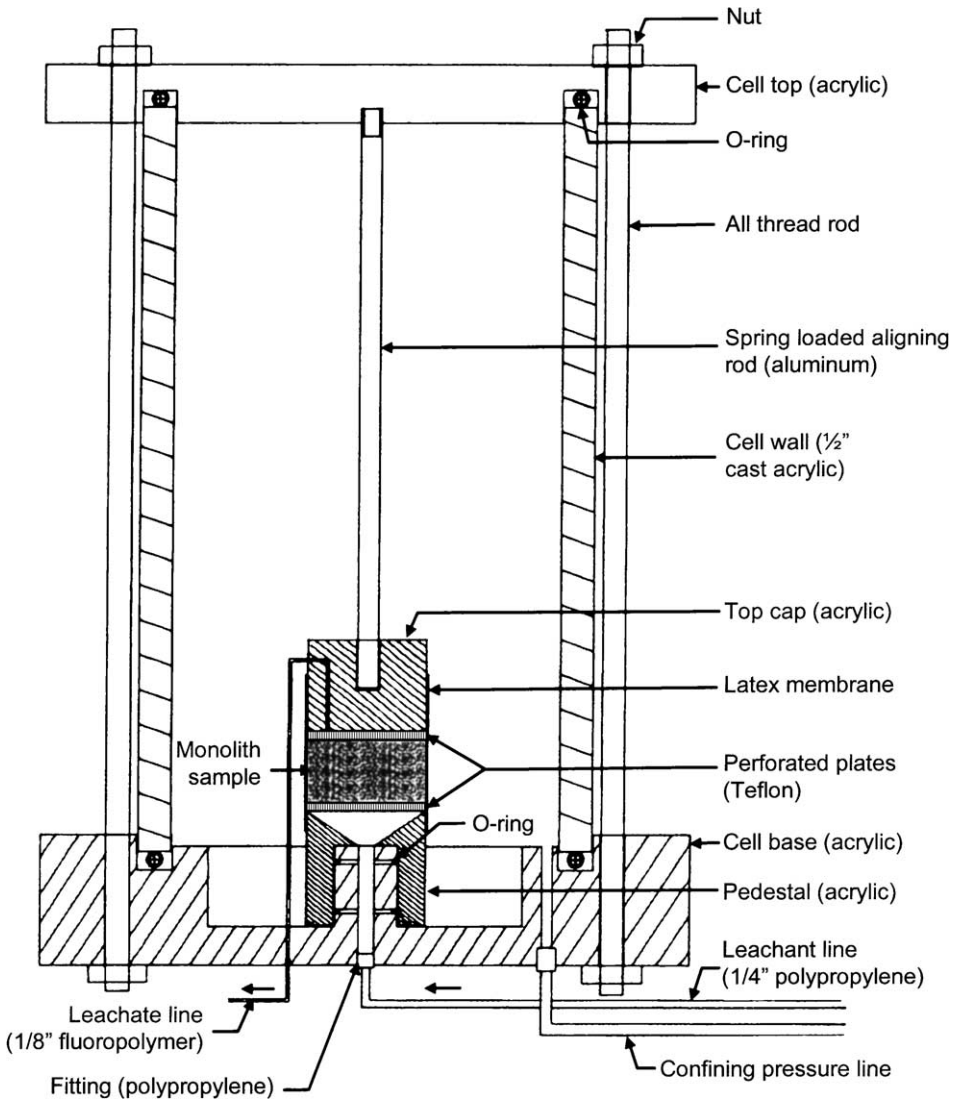

Fig. 1. Schematic diagram of modified triaxial cell used in flow-through leaching tests on monolithic samples.

a peristaltic pump. Table 3 shows the operating parameters for tests C1 and C2. The s/s treated material used in column tests was crushed to pass through a 9.5-mm standard sieve. A total of 90% of the crushed material mass was contained in particles larger than 0.8 mm. The porosity of each column pack (i.e. the volume fraction between the particles) was determined from the mass of packed solids, the bulk density of uncrushed material and the column volume. The difference in porosity between tests C1 and C2 reflects the difficulty in achieving reproducible column packs.

Table 2
Operating parameters of flow-through leaching tests in modified triaxial cell

Test	Sample diameter (mm)	Sample height (mm)	Leachant injection pressure (kPa)
T1	35	18	319
T2	35	16	382
T3	35	16	207
T4	35	16	207
T5	35	14.6	103

Table 3
Operating parameters of flow-through leaching tests in packed columns

Test	Column inner diameter (mm)	Packing height (mm)	Solids weight (g)	Packing porosity (%)	Mean flow rate[a] (ml/min)
C1	51	202	459.4	36.7	0.145
C2	51	202	522.2	28.1	0.208

[a] Before breakthrough of the pH front.

TCLP tests were carried out in triplicate on the crushed material using method 1311 [4]. Extraction fluid #1 was determined to be the required leachant for s/s treated natrojarosite.

Leachate samples were collected in glass containers, filtered through 0.45 μm cellulose acetate membrane syringe filters, and acidified with 2% reagent grade HCl prior to analysis by inductively coupled plasma atomic emission spectroscopy (ICP–AES). Compliance with quality assurance/quality control criteria was verified through analysis of control samples, duplicates, and double distilled water blanks.

2.3. Analytical electron microscopy

Samples of s/s treated waste before and after leaching were impregnated with epoxy resin, polished using kerosene to obtain smooth grain sections without dissolving water-soluble minerals, and coated with carbon. The polished sections were examined with a JEOL JSM 5900 SEM. The elemental composition of the mineral phases was determined by EDX using an Oxford Link ISIS System calibrated using a pyrite standard for Fe and S, a wollastonite standard for Ca, an orthoclase standard for Al, K and Na, a garnet standard for Mg and Si, a chalcopyrite standard for Cu, a galena standard for Pb, and a sphalerite standard for Zn.

3. Results

3.1. Evolution of leachate flow rates and pH

Fig. 2 shows the normalized volume of leachate as a function of time for two typical triaxial tests (T4 and T5) and one column test (C1). One normalized volume (1 NV) of

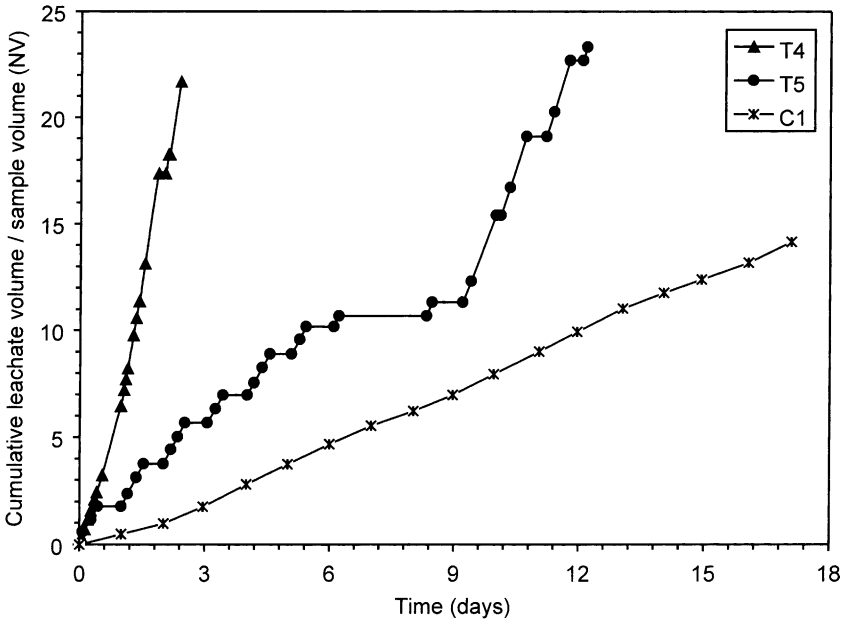

Fig. 2. Cumulative NV of leachate vs. time for triaxial tests T4 and T5 and column test C1.

leachate is defined as 1 cm^3 of leachate per cm^3 of s/s treated material. Leachant injection was not continuous for test T5: normally, the leachant solution was injected during the day and interrupted at night. Near the middle of the test, leachant injection was interrupted for 2 continuous days.

The leachate Darcy velocities (i.e. the volumetric flow rate divided by the cross-sectional area of the sample) are plotted as a function of normalized leachate volume in the upper-half of Fig. 3 for tests T4 and T5. Following the start of the tests, Darcy velocities were nearly steady. After a certain volume of leachate (lower for test T4 than for T5), the Darcy velocities began to increase quickly. The overall permeability of the treated sample increased from 8.7×10^{-10} to 1.9×10^{-9} m/s during test T4 and from 9.0×10^{-10} to 1.6×10^{-9} m/s during test T5.

The evolution of leachate pH versus normalized leachate volume shown in the lower-half of Fig. 3 for tests T4 and T5 was consistent with the advancement of a pH front from the inlet toward the outlet of the treated waste samples during triaxial tests. Breakthrough of the pH front at the outlet face of the samples resulted in a leachate pH drop from pH > 9 to pH < 7. The front was sharper at the higher leachant flow rate (T4). The same behavior was observed in column tests. Before breakthrough, metal ion mobilized upstream of front (where pH was acid to neutral) could re-precipitate as hydroxides downstream of the front (where pH was alkaline). The build-up of metal precipitates in the pores downstream of the pH front may have created a zone of reduced permeability moving with the front. However, other co-occurring mechanisms such as micro-fracturing and progressive dissolution of the C–S–H gel and gypsum in the treated waste had an opposite effect on permeability. Darcy

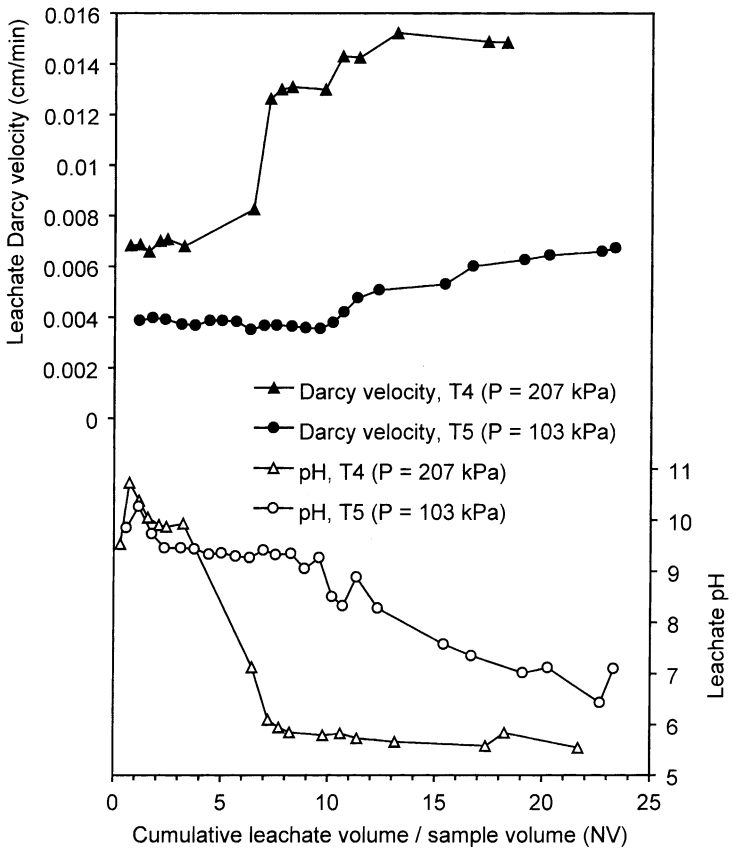

Fig. 3. Leachate Darcy velocities and pH vs. normalized leachate volume for triaxial tests T4 and T5.

velocity trends before pH front breakthrough suggest that the effect of precipitates build-up and the effect of micro-fracturing and matrix dissolution nearly compensated each other in tests T4 and T5. When breakthrough of the pH front occurred, the resistance to flow caused by the build-up of precipitates downstream of the front disappeared. This likely explains why the fast increase in leachate Darcy velocity coincided with the drop in leachate pH in both tests.

3.2. Factors controlling pH front breakthrough

Fig. 4 plots the NV of leachate at breakthrough of the pH front, NV_{bt}, versus the residence time of the leaching solution in the treated material for all triaxial and packed column tests. The calculation of residence times is detailed in Appendix A. Although tests T3 and T4 were replicates, their residence times were significantly different (71 and 138 min, respectively). This difference indicates that the permeability of the treated waste sample was higher in test T3 than in T4, in spite of the fact that both samples

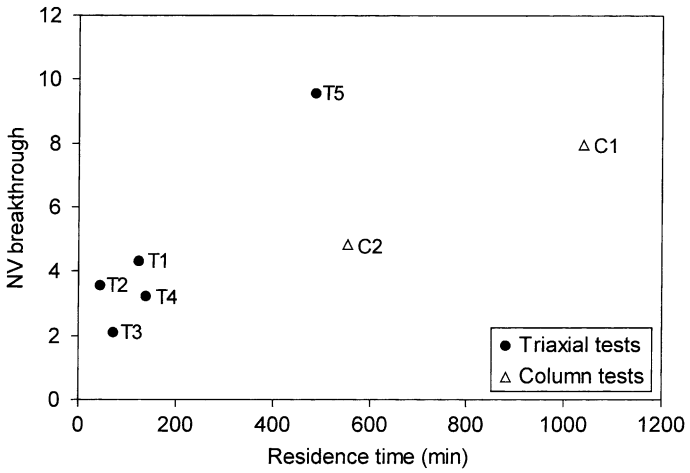

Fig. 4. NV of leachate recovered at pH front breakthrough vs. leachate residence time for five triaxial tests and two column tests. Operating parameters for all tests are given in Tables 2 and 3.

originated from the same batch of treated natrojarosite and were cured under the same conditions.

NV_{bt} increased with residence time in triaxial and column tests. This observation can be explained as follows. When the leachant started flowing through the treated waste, it preferentially reacted with the alkalinity immediately adjacent to the flow paths. Later in the tests, neutralization of the leachant became limited by the diffusion rate of acid and basic species through material from which alkalinity had already been depleted (Barna et al. [12]). Hence, longer residence times allowed alkalinity located further away from the flow paths to react with the leachant. This resulted in more alkalinity being effectively available to neutralize the leachant. Consequently, pH breakthrough was delayed to higher NV values.

In the following, we call "effective alkalinity" the amount of alkalinity that is depleted from the treated waste samples before breakthrough of the pH front. For long enough residence times, as the effective alkalinity approaches the total available alkalinity, NV_{bt} is expected to tend toward an asymptotic value. However, we were not able to demonstrate this behavior due the limited number of experiments with high residence times.

For a given residence time, NV_{bt} values were lower in column tests than in triaxial tests. This is not surprising considering that in column tests the leachant flowed around the particles of treated waste, whereas, in triaxial tests the leachant flow was through the internal porosity of the monolithic samples. Hence, the distances over which chemical species were transported by diffusion before participating in neutralization reactions were smaller in triaxial tests. This led to larger effective alkalinities for monolithic samples compared to crushed samples.

The increase is pH between NV = 10.7 and 11.3 observed in test T5 (Fig. 3) was due to the fact that flow was stopped for 2 days at NV = 10.7, thus resulting in a very long residence time for the leachate sample corresponding to NV = 11.3.

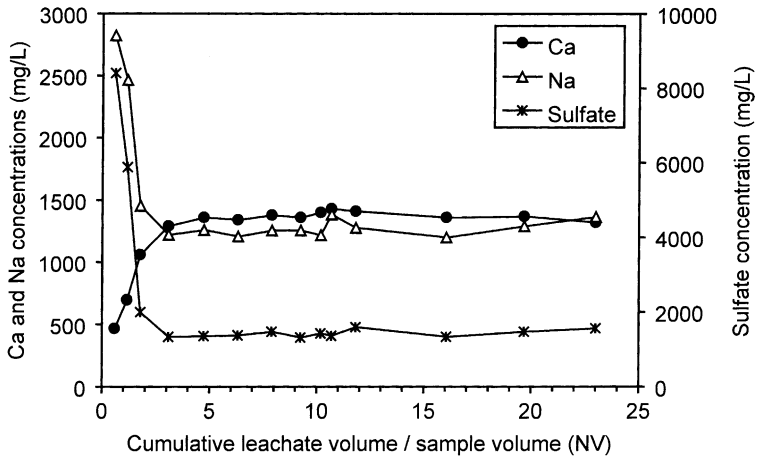

Fig. 5. Evolution of Ca, Na and sulfate concentrations in the leachate of triaxial test T5.

3.3. Leaching of major ions

Figs. 5 and 6 show the evolution of Ca, Na and sulfate concentrations in the leachate of tests T5 and C1, respectively, versus normalized leachate volume. Na and sulfate exhibited similar leaching patterns: their concentrations decreased from initially high values to stable levels. By contrast, Ca concentrations increased toward a plateau at approximately 1500 mg/l. It is noteworthy that stable concentrations were reached after approximately 3 NV of leachate in test T5, but only after approximately 8 NV of leachate in test C1. This result can be attributed to the greater effect of longitudinal hydrodynamic dispersion

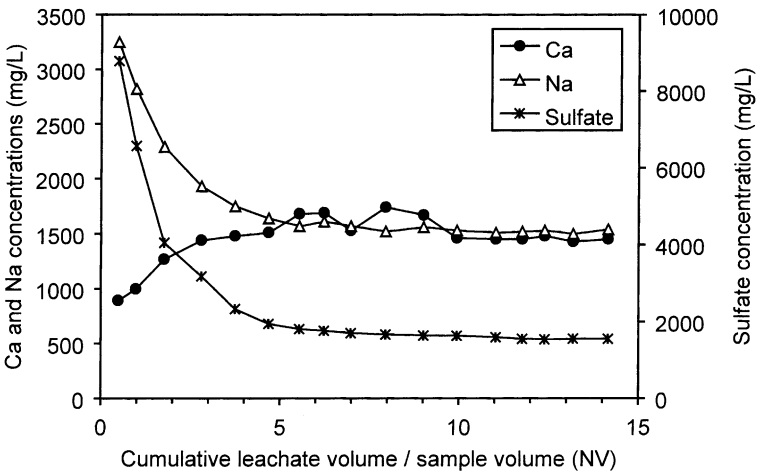

Fig. 6. Evolution of Ca, Na and sulfate concentrations in the leachate of column test C1.

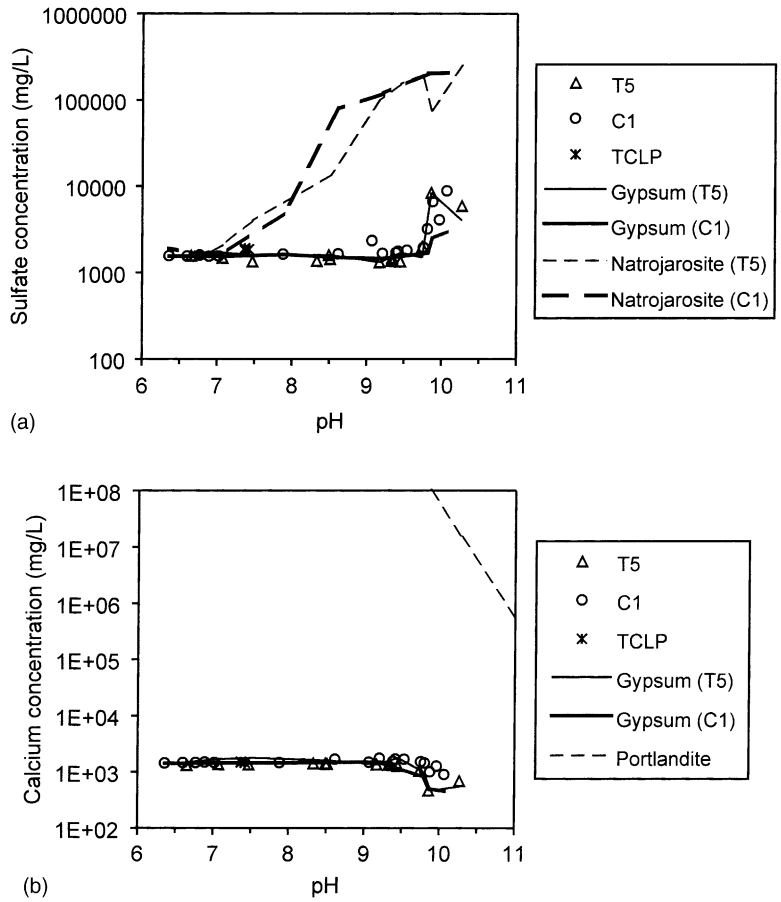

Fig. 7. Measured concentrations of (a) sulfate and (b) calcium in the leachates of tests T5, C1, and TCLP as a function of pH. Predicted equilibrium concentrations with gypsum, natrojarosite, and portlandite were calculated using Visual MINTEQ.

in column tests compared to triaxial tests, since the columns were much longer than the monolithic samples in the direction of flow.

Elevated sulfate concentrations in the early leachate samples likely resulted from the displacement of interstitial solution rich in sulfate and the simultaneous dissolution of gypsum. Fig. 7a plots sulfate concentrations versus leachate pH for tests T5 and C1. The geochemical equilibrium Software Visual MINTEQ [13] was used to calculate sulfate concentrations in equilibrium with gypsum and natrojarosite within the same pH range. Comparison of measured and calculated sulfate concentrations shows that the leachates were at equilibrium with respect to gypsum throughout the leaching tests. Undersaturation with respect to natrojarosite at pH > 7 suggests that natrojarosite and, therefore, heavy metal impurities contained in the natrojarosite crystals, remained shielded from the leaching solution downstream of the pH front. Microscopic analyses (as mentioned later) showed that the C–S–H

gel surrounding natrojarosite crystals accounted for this "shielding" effect. Below pH 7, however, the leachates reached equilibrium with respect to natrojarosite, thus implying that the C–S–H gel was not effective in shielding natrojarosite crystals upstream of the pH front.

Fig. 7b shows that Ca concentrations were controlled by the solubility of gypsum throughout the pH range of the leaching tests. The concurrent increase in Ca concentrations and decrease in sulfate concentrations after the start of the tests is consistent with the $\{SO_4^{2-}\}\{Ca^{2+}\}$ activity product remaining constant. Part of the released Ca originated from the dissolution of cement hydration products. Leachates were undersaturated with respect to portlandite [$Ca(OH)_2$] throughout the leaching tests, thus indicating that portlandite is not a product of cement hydration in treated natrojarosite waste. Butcher et al. [6] also reported an almost complete absence of portlandite in a metal waste treated with high waste to cement ratios.

Stable Na concentrations were close to the Na concentration in the leachant solution (1478 mg/l). The high Na concentrations measured at the start of the leaching tests were mostly due to the leaching of Na originally present in cement (OPC contained 1814 μg/g of Na). This explanation was corroborated by measurements of similarly high initial Na concentrations during further flow-through leaching tests carried out on metal nitrate sludges treated with OPC. These sludges were devoid of Na before s/s treatment.

3.4. Leaching of heavy metals

Figs. 8 and 9 show the evolution of heavy metal concentrations in the leachates of tests T5 and C1, respectively, as a function of normalized leachate volume. Elevated concentrations of Cu (17.6 mg/l), Zn (5.8 mg/l) and Pb (3.0 mg/l) were measured immediately after the start of test T5. These concentrations decreased with increasing leachate volume: Pb and

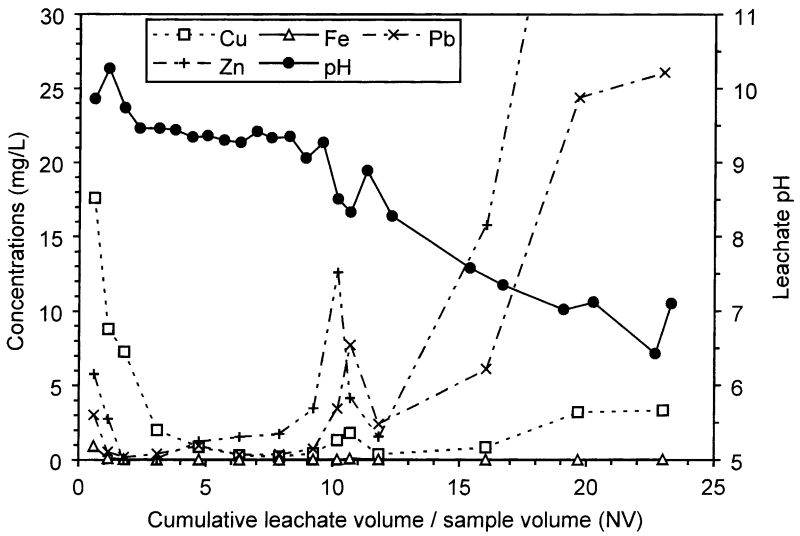

Fig. 8. Evolution of Cu, Fe, Pb and Zn concentrations and pH in the leachate during triaxial test T5.

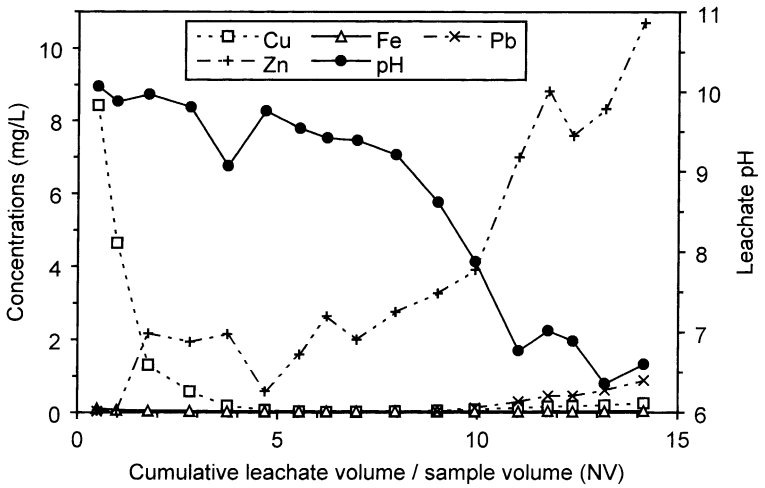

Fig. 9. Evolution of Cu, Fe, Pb and Zn concentrations and pH in the leachate during column test C1.

Zn reached low values (0.19 and 0.02 mg/l, respectively) after 1.8 NV of leachate. The Cu concentration decreased more gradually than the other metals and reached a minimum of 0.023 mg/l after 6.32 NV of leachate. Similar trends were observed in all other triaxial tests (T1–T4). Column tests yielded similar leaching trends for heavy metals. In test C1, Cu was initially high (8.4 mg/l) and reached a minimum of 0.014 mg/l after 6.23 NV of leachate. After breakthrough of the pH front, heavy metal concentrations increased substantially in both triaxial and column tests as the leachate pH dropped.

Fig. 10a–c plot the concentrations of Cu, Pb, and Zn versus leachate pH for tests T4, T5, C1 and C2. These concentrations are compared to their predicted values calculated using Visual MINTEQ assuming chemical equilibrium with metal hydroxides in a 5880 mg/l acetate solution. The leachates were generally oversaturated with respect to their metal hydroxides in the range of pH values measured before breakthrough of the pH front (9–11). The elevated metal concentrations measured at alkaline pH immediately after the start of the leaching tests (enclosed by dotted lines in Fig. 10a–c) may have resulted from the large buffering capacity of the acetic acid/sodium acetate leachant solution. As the acid leachant entered the pores of the treated waste, it was able to leach significant amounts of metals before enough alkalinity reacted to raise the pH to alkaline values. Because of this initial "acid shock", low pH conditions may have existed within a significant length of the monoliths and columns immediately after the start of the tests. As the leachant advanced further through the sample, its acid buffering capacity was eventually neutralized by reacting with alkaline hydration products, as demonstrated by the fact that the pH of the early leachates was alkaline. However, because the slow kinetics of metal precipitation compared to the residence time of the leaching solution in the treated waste, supersaturated metal concentrations could be transported through the samples and report to the leachate. Hidmi and Edwards [14] showed that several hundred hours can be required to reach equilibrium solubility values for Cu precipitating as $Cu(OH)_2$. As leaching progressed, alkaline hydration products continued

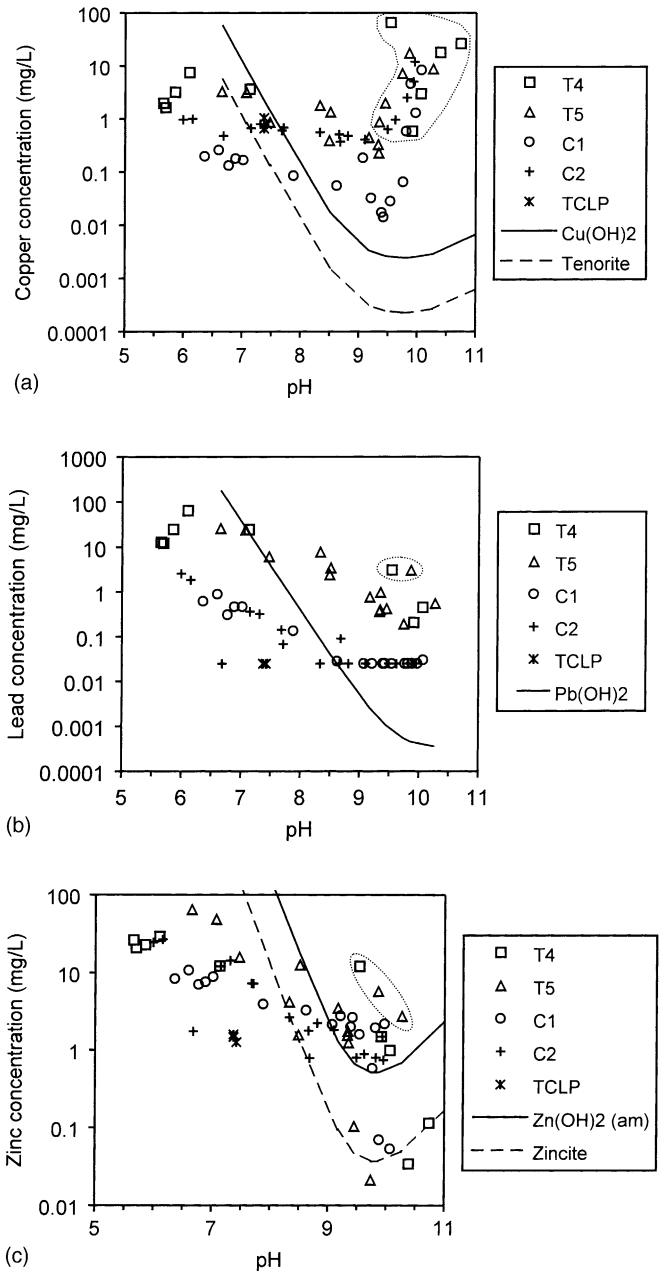

Fig. 10. Measured concentrations of (a) Cu, (b) Pb, and (c) Zn in the leachates of tests T4, T5, C1, C2, and TCLP as a function of pH. Predicted equilibrium concentrations with hydroxide minerals were calculated using Visual MINTEQ. Data points corresponding to elevated metal concentrations measured immediately after the start of the flow-through leaching tests are enclosed by dotted lines.

to dissolve throughout the s/s treated sample, thus increasing the pH of the pore solution in areas affected by the initial "acid shock". This caused metal concentrations in the leachates to decrease to the low values measured some time after the start of the tests. Entrainment of colloidal particles of treated material by the leaching solution may also have contributed to the high initial metal concentrations, as suggested in Butcher et al. [6].

Except for the high initial values, heavy metal concentrations displayed a clear increasing trend with decreasing leachate pH. In the pH range after pH front breakthrough (pH < 7), the leachates became undersaturated with respect to metal hydroxides. During that stage, metal concentrations were probably limited by the dissolution kinetics and the diffusion rates of metals from the solid to the leaching solution.

Leachate concentrations of Cu and Pb were lower in column tests than in triaxial tests, both before and after breakthrough of the pH front. This is consistent with longer diffusion paths in column tests, as previously discussed. By contrast, the leaching behavior of Zn was similar in column and triaxial tests. The Zn concentration may have been controlled by the numerous zinc ferrite ($ZnFe_2O_4$) grains present in the treated natrojarosite. SEM–EDX analyses (as mentioned later) revealed that these grains were almost free of C–S–H coating. The leaching of zinc ferrite grains located on the edge of particles of treated material would not have been diffusion limited and could explain the similarity between the results of column and triaxial tests for Zn.

Fig. 11 plots the cumulative percentages of Cu, Pb and Zn leached during tests T5 and C1. Only a very small percentage of the heavy metals initially contained in the treated natrojarosite were leached before breakthrough of the pH front: 1.64% Cu, 0.016% Pb and 0.090% Zn in test T5; 0.52% Cu, 0.00004% Pb and 0.075% Zn in test C1.

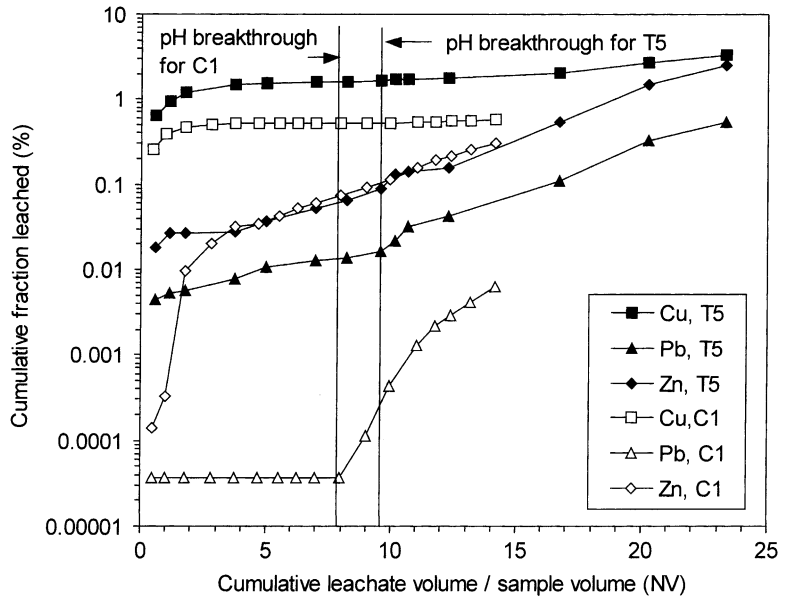

Fig. 11. Cumulative percentage of heavy metals leached during tests T5 and C1 vs. leachate NV.

Table 4
Results of TCLP test

Parameter	Concentration[a] (mg/l)	Percent leached[a]
Ca	1493	57.6
Cd	0.070	1.63
Cu	0.833	1.83
Fe	0.044	0.0005
Pb	<0.025	<0.0023
SO_4	1862	19.8
Zn	1.44	0.276
pH	7.39	

[a] Averages over triplicate tests.

3.5. Leaching behavior during TCLP

The average concentrations of several elements in the TCLP extracts of treated natrojarosite are presented in Table 4. TCLP extractions were carried out at a leachate:sample volume ratio of 35.2 (as calculated from the liquid:solid mass ratio of 20 required by the TCLP procedure and the bulk density of the treated material). It is noteworthy that the TCLP extracts had a higher average pH (7.39) than the leachates of flow-through leaching tests at a similar leachate:sample volume ratio, as can be seen by extrapolating the pH data on Figs. 8 and 9. This result is a consequence of the fact that the TCLP is a static leaching test and, therefore, all the alkalinity contained in the solid sample is available to neutralize the leachant. By contrast, during flow-through leaching tests, part of the alkalinity initially present in the treated waste was dissolved in the leachate "downstream" of the pH front and was, therefore, removed from the material before having had the opportunity to react with the acidity of the leachant. This alkalinity "washout" effect associated with flow-through leaching tests was also pointed out by Yan et al. [15].

The sulfate concentration in the TCLP extracts was at near equilibrium with respect to natrojarosite (Fig. 7a). This suggests that the natrojarosite crystals were no longer effectively shielded with C–S–H gel by the end of the TCLP tests. Gypsum was the solubility controlling phase for Ca (Fig. 7b). Cu concentrations in the TCLP extracts were between the predicted solubilities of $Cu(OH)_2$ and tenorite (CuO) (Fig. 10a). Fig. 10b and c shows that Zn and Pb concentrations were well below those predicted by the solubility of $Pb(OH)_2$, $Zn(OH)_2$ (am) and zincite (ZnO). It is, therefore, unlikely that Pb or Zn were present in the treated material in these mineral forms. Our results are in agreement with those reported in Li et al. [16] for Cu and Zn. Cumulative percentages of heavy metals leached during TCLP extractions were small (Table 4).

3.6. Analytical electron microscopy

Fig. 12 shows a typical backscattered photomicrograph of a section of treated natrojarosite waste before leaching. Three main features are clearly visible: (1) natrojarosite crystals coated with C–S–H gel; (2) gypsum; and (3) a phase rich in Zn and Fe which was identified

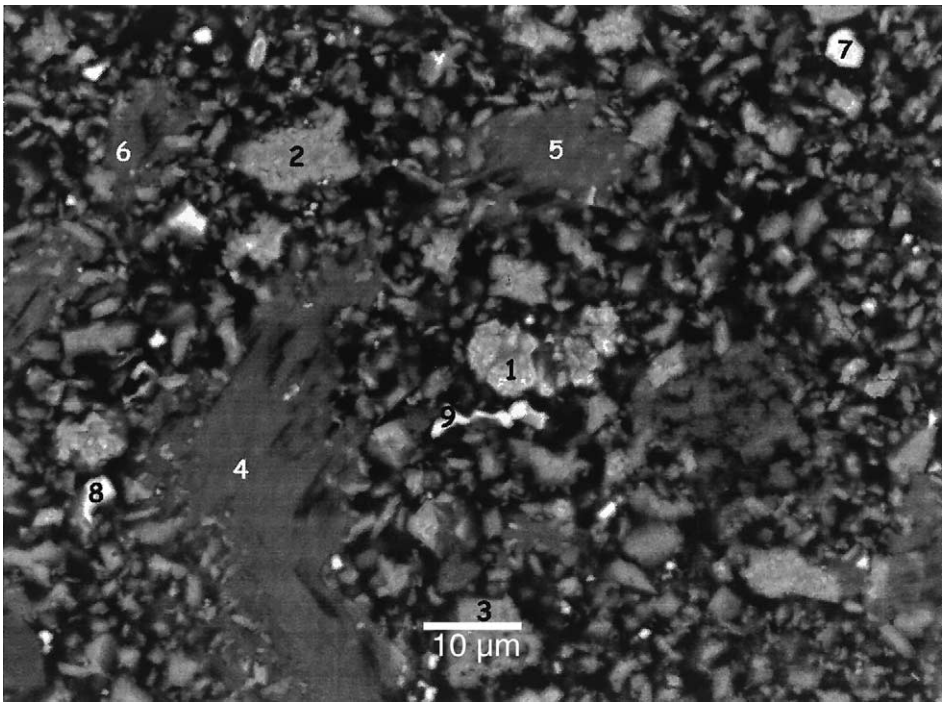

Fig. 12. Typical backscattered photomicrograph of treated natrojarosite waste before leaching: (1–3) natrojarosite coated with C–S–H gel; (4–6) gypsum; and (7–9) zinc ferrite.

as zinc ferrite. The elemental composition of these features was evaluated by averaging several EDX analyses carried out at several locations on polished sections. The results are given in Table 5 and are similar to those reported in Chen and Dutrizac [2]. The average Ca and Si contents of natrojarosite crystals, 2.04 and 1.41 wt.%, indicate that these crystals were coated with cement hydration products, most likely C–S–H gel. Some variability was present in the amount of coating, as shown by the standard deviation (S.D.) of the Ca concentration (0.72 wt.%). The spatial resolution of EDX (typically 2 μm) did not permit separate analyses of the C–S–H gel and the underlying natrojarosite crystals. Therefore, the extent to which cement hydration products actually reacted with natrojarosite crystals by opposition to simple encapsulation could not be determined by this technique.

Natrojarosite crystals coated with C–S–H contained significant amounts of Zn and Pb (1.42 and 6.27 wt.% on average, respectively). Zn and Pb were detected at low concentrations (0.46 and 1.22 wt.%, respectively) in gypsum in one and two EDX analyses out of five, respectively. Hence, the dissolution of gypsum may have contributed to some extent to the leaching behavior of Pb and Zn. The low Ca concentration (0.32 wt.% on average) in zinc ferrite grains suggests that these grains were poorly coated by cement hydration products.

Fig. 13 shows a backscattered photomicrograph of monolithic material after leaching (T5). Large areas of gypsum were still visible, indicating that the initial gypsum was not

Table 5
X-ray microanalysis results for treated natrojarosite waste before leaching (all concentrations are in wt.%)

	Natrojarosite	Gypsum	Zinc ferrite
	No. of analyses		
	12	5	4
Na	3.24 ± 0.52[a]	<0.62	2.54 ± 0.27
Mg	<0.28[b]	–	–
Al	<0.30	–	<0.22
Si	1.41 ± 0.20	0.21 ± 0.09	0.24 ± 0.10
S	9.16 ± 1.12	19.9 ± 1.4	<0.41
K	<0.15	<0.20	–
Ca	2.04 ± 0.72	24.2 ± 2.1	0.32 ± 0.20
Fe	29.9 ± 2.9	1.44 ± 1.07	43.7 ± 2.8
Cu	<1.01	–	<0.48
Zn	1.42 ± 1.09	<0.46	24.2 ± 1.5
Pb	6.27 ± 3.76	<1.22	–

[a] S.D.
[b] The sign "<" indicates that the particular element was below the detection limit for one or more analyses. The reported concentration corresponds to the average of analyses above the detection limit.

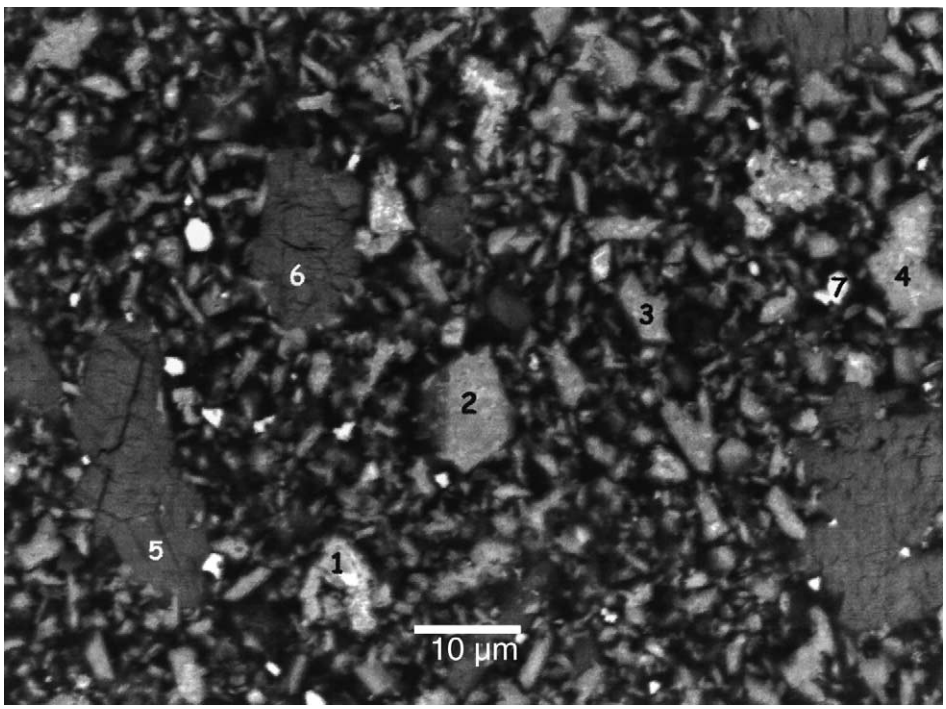

Fig. 13. Typical backscattered photomicrograph of a monolith of treated natrojarosite waste after flow-through leaching in a modified triaxial cell (T5): (1–4) natrojarosite; (5–6) gypsum; and (7) zinc ferrite.

Table 6
X-ray microanalysis results for natrojarosite crystals in treated waste after flow-through leaching (all concentrations are in wt.%)

	Packed column sample (C1)	Monolith sample (T5)
	No. of analyses	
	10	12
Na	2.87 ± 0.73	3.17 ± 0.78
Mg	<0.21	<0.26
Al	<0.20	<0.35
Si	1.29 ± 0.40	1.97 ± 0.64
S	8.95 ± 1.66	9.27 ± 1.40
K	–	<0.15
Ca	1.49 ± 0.52	0.55 ± 0.31
Fe	30.4 ± 2.0	32.1 ± 1.9
Cu	<0.32	<0.42
Zn	1.13 ± 0.49	1.53 ± 0.78
Pb	4.63 ± 1.56	5.95 ± 1.28

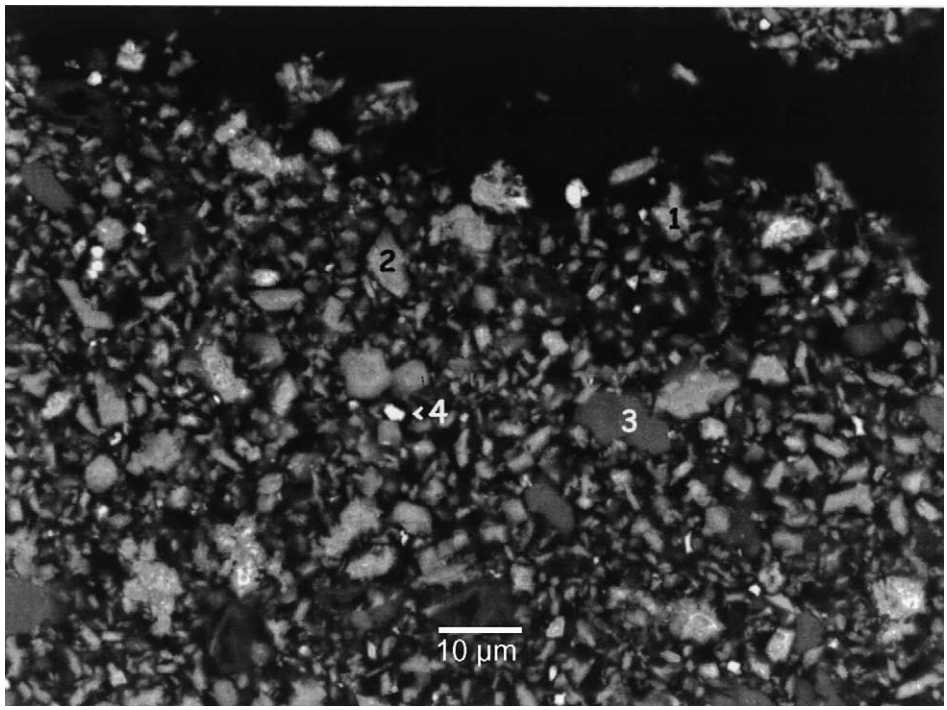

Fig. 14. Typical backscattered photomicrograph of the edge of a grain of treated natrojarosite waste after flow-through leaching in a packed column (C1): (1–2) natrojarosite; (3) gypsum; and (4) zinc ferrite.

completely dissolved during leaching. The remaining gypsum shows ample evidence of weathering (cracks) resulting from the leaching process. The average composition of natrojarosite crystals after test T5 is given in Table 6. The difference between average Ca concentrations of natrojarosite crystals before and after leaching (2.04 and 0.55 wt.%, respectively) was found to be statistically significant at a confidence level >99.99% using a *t*-test. The low Ca content after leaching indicates that the dissolution of the C–S–H gel was very advanced by the end of test T5, in agreement with the results of geochemical equilibrium calculations presented earlier.

Fig. 14 shows the edge of a grain of treated waste after leaching in a packed column (C1). The composition of natrojarosite crystals after test C1 (last column of Table 6) revealed a significantly higher average Ca concentration (1.49 wt.%) than after test T5. However, this average was still significantly lower (at a 97% confidence level) than that measured before leaching. It was also found that the Ca concentration could vary dramatically between two natrojarosite crystals separated by only a few μm. For example, the Ca concentrations in crystals noted 1 and 2 on Fig. 14 were 0.68 and 2.11 wt.%, respectively. No correlation was found between the Ca content of natrojarosite crystals and the distance separating the crystals from the edge of the grains. The lower dissolution of the C–S–H gel in test C1 compared to test T5 can be attributed to the lower NV of leachant used in test C1 compared to test T5, combined with the fact that monolithic samples have a larger effective alkalinity than crushed samples, as shown earlier.

4. Discussion

4.1. Modeling of flow-through leaching

At the present time, no published mathematical model is available to scale-up the results of laboratory flow-through leaching tests to the field situation. Our results indicate that such a model would need to take into consideration both physical and chemical mechanisms in order to predict leachate quality as a function of time. Existing leaching models that consider chemical/physical coupling (e.g. Barna et al. [12], Moszkowicz et al. [17], Baker and Bishop [18], Hinsenveld and Bishop [19], Batchelor [20]) have been devised for batch leaching where a monolithic sample is immersed in a leachant solution. In batch leaching, the leachant does not flow through the treated waste, and diffusion is the only mechanism of contaminant transport within the material. Hence, the corresponding models do not account for convective contaminant transport and variations in chemical conditions along the direction of flow.

In the field, the buffering capacity of the leachant (acid rain) is much lower than that of the buffered acetic acid/sodium acetate solution used in our tests. Consequently, the initial "acid shock" effect is much reduced, and heavy metal concentrations in the leachate are anticipated to remain low as long as the pH front has not broken through. A rough prediction of the evolution of field leachate quality can, therefore, be obtained by modeling the advance of the pH front, which is in turn controlled by the progressive depletion of the alkalinity in the treated waste. In the following, we develop a preliminary scale-up model of alkalinity depletion for the flow-through leaching process.

4.2. Model of alkalinity depletion for flow-through leaching

The purpose of this model is to predict the time to breakthrough of the pH front by providing a simplified mathematical description of the mechanisms of alkalinity depletion in the treated waste. The alkalinity depletion rate, α, is defined as the alkalinity removed from the treated waste per unit volume of leachant flowing through the treated waste. The units of α are, therefore, eq/l. For a leachant consisting of a buffered acetic acid/sodium acetate solution, α is given by:

$$\alpha = [HAc]_1 - [HAc]_2 + [OH^-]_2 \tag{1}$$

where $[HAc]_1$ and $[HAc]_2$ are the acetic acid concentrations in the leachant and leachate, respectively, and $[OH^-]_2$ is the hydroxide ion concentration in the leachate. Concentrations have units of mol/l. The difference between the first two terms on the right hand side of Eq. (1) corresponds to the alkalinity depletion caused by the following neutralization reaction:

$$HAc + OH^- \rightarrow Ac^- + H_2O \tag{2}$$

The last term on the right hand side of Eq. (1) accounts for alkalinity that is transferred to the leachate but does not react with acid species in the leachant (i.e. the alkalinity "washout" effect). The chemical equilibria associated with the dissociation of acetic acid and water are, respectively, as follows:

$$\frac{[Ac^-]_2[H^+]_2}{[HAc]_2} = K_a \tag{3}$$

and

$$[OH^-]_2[H^+]_2 = K_w \tag{4}$$

where $[Ac^-]_2$ and $[H^+]_2$ are the acetate and hydronium ion concentrations in the leachate, respectively. K_a is the dissociation constant of acetic acid (1.75×10^{-5} at 25 °C) and K_w is the ionization constant of water (1×10^{-14} at 25 °C). Combining Eqs. (1), (3) and (4) yields:

$$\alpha = \frac{([Ac^-]_1 + [HAc]_1)K_a}{(K_a + 10^{-pH_2})} - [Ac^-]_1 + 10^{pH_2}K_w \tag{5}$$

where pH_1 and pH_2 refer to the leachant and leachate solutions, respectively. Eq. (5) is only valid when the leachant is a buffered solution of a weak acid and base. For a leachant consisting of a solution of one or several strong acids (e.g. HNO_3 and H_2SO_4), the alkalinity depletion rate is given by:

$$\alpha = [H^+]_1 - [H^+]_2 + [OH^-]_2 \tag{6}$$

where $[H^+]_1$ is the hydronium ion concentration in the leachant. The difference between the first two terms on the right hand side of Eq. (6) accounts for the neutralization reaction:

$$H^+ + OH^- \rightarrow H_2O \tag{7}$$

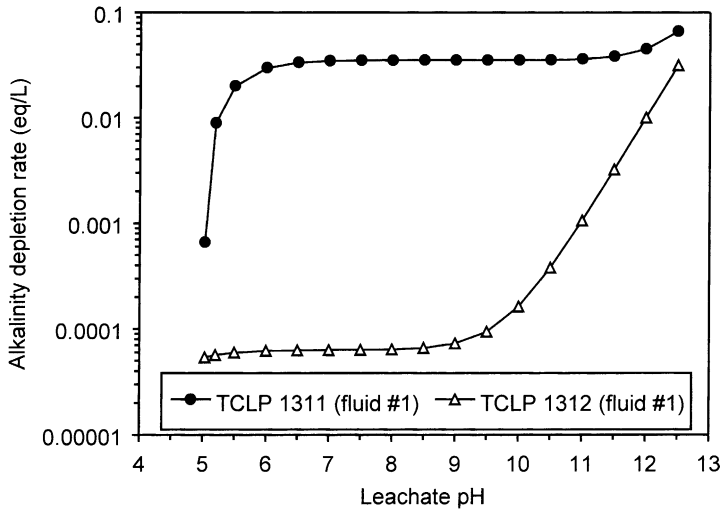

Fig. 15. Alkalinity depletion rate vs. leachate pH for TCLP 1311 and 1312 leachants.

Combining Eqs. (4) and (6) gives:

$$\alpha = 10^{-\mathrm{pH}_1} - 10^{-\mathrm{pH}_2} + 10^{\mathrm{pH}_2} K_\mathrm{w} \tag{8}$$

Fig. 15 plots the alkalinity depletion rate versus leachate pH for the following two common leachants:

- extraction fluid #1 of TCLP method 1311, which is a buffered solution of acetic acid and sodium acetate at $\mathrm{pH}_1 = 4.93 \pm 0.05$ [4];
- extraction fluid #2 of TCLP method 1312, which is a dilute solution of sulfuric and nitric acids at $\mathrm{pH}_1 = 4.20 \pm 0.05$ [4] and simulates acid rain east of the Mississippi river.

The alkalinity depletion rate for the TCLP 1311 leachant is quite stable at 0.035 eq/l in the leachate pH range 7–10.5. Therefore, α is equal to 0.035 eq/l in all our flow-through leaching tests for the entire period preceding breakthrough of the pH front. The α-values are smaller for the TCLP 1312 leachant than for the TCLP 1311 leachant. However, the difference between the two leachants decreases at high pH. For the range of leachate pH values measured in our tests before breakthrough of the pH front (9–10.5), α of the TCLP 1312 leachant is less than 3.8×10^{-4} eq/l.

The effective alkalinity per unit volume of treated waste, A_e (eq/m^3), is defined as the alkalinity that is depleted prior to the breakthrough of the pH front (or more generally, as the alkalinity depletion before the leachate pH reaches a limit below which heavy metal concentrations in the leachate are deemed unacceptable). A_e is given by:

$$A_\mathrm{e} = \frac{1000\alpha V_{\mathrm{l,bt}}}{V_\mathrm{w}} = 1000\alpha \mathrm{N} V_\mathrm{bt} \tag{9}$$

Table 7
Model parameter estimates based on the results of flow-through tests

Test	NV_{bt}	α (TCLP 1311 fluid #1) (eq/l)	A_e (eq/m^3)
T5	9.6	0.035	336
C1	7.9	0.035	277

where $V_{l,bt}$ (m^3) and NV_{bt} are, respectively, the cumulative leachate volume and the number of NV of leachate collected when breakthrough of the pH front occurs. V_w (m^3) is the volume of the treated waste. We also have as follows:

$$V_{l,bt} = \Omega v t_{bt} \tag{10}$$

and

$$V_w = \Omega L \tag{11}$$

where t_{bt} (s) is the time to breakthrough of the pH front, Ω (m^2) is the cross-sectional area of the waste perpendicular to flow, v (m/s) is the Darcy velocity of the leaching solution, and L (m) is the height of treated waste. Combining Eqs. (9)–(11) yields:

$$t_{bt} = \frac{A_e L}{1000 \alpha v} \tag{12}$$

This equation gives the time to breakthrough of the pH front as a function of the effective alkalinity of the treated waste, the height of treated waste, the alkalinity depletion rate, and the Darcy velocity of the leaching solution.

4.3. Prediction of time to breakthrough of the pH front for field conditions

Using Eq. (9), estimates of the effective alkalinity A_e for treated natrojarosite were calculated from the values of NV_{bt} obtained in tests T5 and C1 (Table 7). These two tests were selected because they involved long leachant residence times and were, therefore, considered the most representative of actual field conditions.

In the field the leachant is acid rain, which is approximated by the TCLP 1312 leachant. Using Eq. (12), the time to breakthrough of the pH front in the field was predicted for infiltration of acid rain through a monolith-type treated material ($A_e = 336$ eq/m^3, similar to test T5) and through treated material that is greatly cracked and fractured due to weathering ($A_e = 277$ eq/m^3, similar to test C1). The results for a 10 m high heap and an infiltration

Table 8
Predictions of time to breakthrough of the pH front in the field

Flow regime	A_e (eq/m^3)	v (m/s)	L (m)	Acid rain α (eq/l)	t_{bt} (year)
Infiltration through monolith-type material	336	3.17×10^{-8}	10	3.8×10^{-4}	8840
Infiltration through cracked and fractured material	277	3.17×10^{-8}	10	3.8×10^{-4}	7290

rate equal to 1000 mm per year ($v = 3.17 \times 10^{-8}$ m/s) are shown in Table 8. The selected infiltration rate is an overestimate and provides a worst-case scenario. In practice, only a small fraction of natural precipitation flows through the treated waste: the majority flows on the surface of the material toward collecting ditches. Breakthrough of the pH front in the field is predicted to occur after 8840 and 7290 years for flow through monolith-type and severely weathered materials, respectively.

The model presented above can only be used to predict times to breakthrough of the pH front; it does not predict solute concentrations in the leachate. It is also important to point out that concentrations measured in the leachates of our flow-through tests after pH front breakthrough may not be representative of those in the field, since buffered acetic acid/sodium acetate solutions have metal complexing properties that are absent in acid rain.

5. Conclusions

The leaching behavior of s/s treated natrojarosite waste was studied by means of flow-through leaching tests on monolithic and crushed samples. The evolution of leachate pH versus leachate volume was consistent with the movement of a pH front within the treated waste. Leachate pH values ranged from 10.5 to 9 before the pH front broke through the outlet face of the samples and decreased to <7 afterwards. The advancement of the pH front was controlled by the progressive depletion of alkalinity in the treated waste. The effective alkalinity was defined as the alkalinity depletion in the period preceding breakthrough of the pH front. Effective alkalinity was found to increase with leachant residence time and was larger for monolithic compared to crushed samples. The overall permeability of the treated material increased after pH front breakthrough.

Geochemical modeling results showed that the C–S–H gel coating on natrojarosite crystals provided an effective shield against direct contact with the leachant downstream of the pH front. However, the leachate was in chemical equilibrium with natrojarosite upstream of the front. Calcium concentrations were controlled by gypsum solubility. Portlandite was found to be absent.

Elevated concentrations of Cu, Pb, and Zn were measured in the early leachates and were attributable to the "acid shock" caused by the initial contact of the buffered acetic acid/sodium acetate leachant with the treated waste. As leaching progressed, heavy metal concentrations decreased but remained oversaturated with respect to metal hydroxides. High initial metal concentrations are not expected in the field, since the buffering capacity of acid rain is very low compared to that of the leachant used in our tests. After breakthrough of the pH front, metal concentrations increased substantially and became controlled by dissolution kinetics and diffusion rates. Cumulative percentages of leached heavy metals were very small.

Static leaching tests such as the TCLP are not suitable for characterizing flow-through leaching behavior, since they do not account for renewal of the leaching solution. Furthermore, static leaching tests overestimate the material's effective alkalinity.

Analytical electron microscopy revealed that the treated waste consisted of natrojarosite crystals coated with C–S–H gel, gypsum, and zinc ferrite grains which were poorly coated by cement hydration products. Leaching caused the dissolution of the C–S–H coating.

Breakthrough of the pH front occurred before all the coating had dissolved. Dissolution of the C–S–H coatings was more advanced in monolithic samples than in crushed samples, consistent with the lower effective alkalinity of the latter.

Our findings demonstrate that suitable mathematical models for scaling-up the results of laboratory flow-through leaching tests must consider both physical and chemical mechanisms. A model has been developed to predict the time to breakthrough of the pH front. The main model parameters are the effective alkalinity of the treated waste and the alkalinity depletion rate. The effective alkalinity depends on the infiltration rate and on whether the flow takes place through a monolith-type or a severely weathered material. The alkalinity depletion rate is determined by the leachant characteristics. The model predicts that for a typical disposal situation, the leachate will remain alkaline and the heavy metals will stay immobilized in the treated waste for many thousands of years.

Acknowledgements

This study was supported by an operating grant from the Natural Sciences and Engineering Research Council of Canada (NSERC). The authors would like to express their appreciation to Noranda Inc., Canadian Electrolytic Zinc (CEZ) for supplying the jarosite waste used in the tests. S. Seyer and L. Rosato of CEZ provided valuable comments regarding the manuscript.

Appendix A. Calculation of residence times in monolithic and crushed samples

For flow through a monolithic sample of s/s treated material, the residence time of the leachant is given by:

$$t_R = \frac{V_P}{Q} \tag{A.1}$$

where V_P is the porous volume of the sample and Q is the volumetric flow rate of the leachant. The porous volume is related to the sample cross-sectional area perpendicular to flow Ω, the sample thickness L, and the material porosity ε by:

$$V_P = \Omega L \varepsilon \tag{A.2}$$

Furthermore, the leachate Darcy velocity is given by:

$$v = \frac{Q}{\Omega} \tag{A.3}$$

Combining Eqs. (A.1)–(A.3) yields:

$$t_R = \frac{\varepsilon L}{v} \tag{A.4}$$

The x-axis on Fig. 4 represents the average residence time before breakthrough of the pH front calculated using the average Darcy velocity before breakthrough of the pH front in

Eq. (A.4). When the leachate flow is not continuous, as in test T5, the average Darcy velocity to be used in Eq. (A.4) is:

$$v = v_f \frac{t_f}{t} \tag{A.5}$$

where v_f is the average Darcy velocity calculated for the periods where the leachate was flowing before breakthrough of the pH front, t_f is the duration of leachate flow before breakthrough, and t is the time at breakthrough (sum of t_f and the duration of flow interruptions).

For flow through a packed column, the average residence time is given by:

$$t_R = \frac{\varepsilon_C L}{v} \tag{A.6}$$

where ε_C is the porosity of the column packing (i.e. the fraction of column volume contained between particles).

References

[1] J.R. Conner, S.L. Hoeffner, Crit. Rev. Environ. Sci. Technol. 28 (4) (1998) 397–462.
[2] T.T. Chen, J.E. Dutrizac, in: Proceedings of the 2nd International Symposium on Extraction and Processing for the Treatment and Minimization of Wastes, Scottsdale, Arizona, 27–30 October 1996.
[3] D. Ivey, Unpublished report, 2000.
[4] Test Methods, for Evaluating Solid Wastes, Physical/Chemical Methods US Environmental Protection Agency, Office of Solid Waste, SW-846 On-line. http://www.epa.gov/epaoswer/hazwaste/test/main.htm (accessed Jan 2002).
[5] N.E. Prange, W.F. Garvey, Waste Testing and Quality Assurance, in: D. Friedman (Ed.), ASTM STP 1062, American Society for Testing and Materials, Philadelphia, Vol. 2, 1990, pp. 217–227.
[6] E.J. Butcher, C.R. Cheeseman, C.J. Sollars, R. Perry, Environ. Technol. 14 (1993) 113–124.
[7] C.S. Poon, Z.Q. Chen, O.W.H. Wai, J. Hazard. Mater. B81 (2001) 179–192.
[8] C.S. Poon, Z.Q. Chen, Chemosphere 38 (3) (1999) 663–680.
[9] C.D. Shackelford, M.J. Glade, Groundwater 35 (2) (1997) 233–242.
[10] P.L. Bishop, Hazard. Waste Hazard. Mater. 5 (2) (1988) 129–143.
[11] P.L. Bishop, in: G.D. Boardman (Ed.), Toxic and Hazardous Wastes. Proceedings of the 8th Mid Atlantic Industrial Waste Conference, Technomic Publishing Company, Lancaster, PA, 1986, pp. 236–252.
[12] R. Barna, F. Sanchez, P. Moszkowicz, J. Méhu, J. Hazard. Mater. 52 (1997) 287–310.
[13] Visual MINTEQ Ver 2.0, http://www.lwr.kth.se/english/OurSoftware/vminteq/index.ht m (accessed Feb 2002).
[14] L. Hidmi, M. Edwards, Environ. Sci. Technol. 33 (1999) 2607–2610.
[15] J. Yan, C. Bäverman, L. Moreno, I. Neretnieks, Sci. Total Environ. 227 (1999) 1–11.
[16] X.D. Li, C.S. Poon, H. Sun, I.M.C. Lo, D.W. Kirk, J. Hazard. Mater. A82 (2001) 215–230.
[17] P. Moszkowicz, F. Sanchez, R. Barna, J. Méhu, Talanta 46 (1998) 375–383.
[18] P.G. Baker, P.L. Bishop, J. Hazard. Mater. 52 (1997) 311–333.
[19] M. Hinsenveld, P.L. Bishop, in: T.M. Gilliam, C.C. Wiles (Eds.), Stabilization and Solidification of Hazardous, Radioactive, and Mixed Wastes, ASTM STP 1240, American Society for Testing and Materials, Vol. 3, 1996, pp. 528–539.
[20] B. Batchelor, Water Sci. Technol. 26 (1/2) (1992) 107–115.